



SHEET CAVITATION NOISE PREDICTION FROM A MARINE PROPELLER

Sandro Ianniello

CNR-INSEAN, Marine Technology Research Institute, Via di Vallerano 139, 00128 Rome, Italy
Email: sandro.ianniello@cnr.it

This paper deals with the numerical prediction of noise from a marine propeller in presence of a sheet cavitation. The analysis is performed by coupling an acoustic code based on the Ffowcs Williams-Hawkings (FWH) equation to a Boundary Element Method (BEM), able to simulate the appearance and the time evolution of a bubble on the blade surface. The noise signature is determined by using a modified version of the well-known Farassat solving formulation 1A, where the integration domain is time-dependent and corresponds to the blade surface *plus* the bubble. The results reveal the expected *true monopole* nature of the body-source, characterized by a significant increase of the noise level and the occurrence of an impulsive waveform (with a higher frequency content) of the acoustic pressure.

1. Introduction

The prediction of the underwater noise from a marine propeller in presence of cavitation phenomena still represents a largely unsolved problem and a bold challenge in the research field of computational fluid dynamics (CFD). The main difficulties arise from the many hydrodynamic aspects of the problem and the limits of the computing resources. The vapor bubble(s) occurring on the surface of a propeller blade (and due to the local decrease of pressure up to the vapor pressure value) evolves in a way strictly dependent on the propeller operating conditions and the surrounding flow. Generally speaking, the bubbles can grow up and change in volume and shape, remain attached to the blade surface or be detached and convected into the downstream flow, occur within the vortex released at blade tip, coalesce with other bubbles and, above all, implode, thus generating intense and localized micro-shockwaves. For a long time, all these phenomena have been observed, studied and even classified into different cavitation types (*bubble, sheet, tip-vortex, cloud*); thus, an extensive bibliography is today available on these issues, dealing with the countless experimental tests performed to examine the related erosive, vibration and acoustic effects. At present, however, CFD is not able to provide any comprehensive simulation of these problems: the difficulties to numerically establish the transition phase and the “trigger” of cavitation, the complex dynamics of the interface, the need of coupling a compressible (vapor) and an incompressible (water) solution of the Navier-Stokes equation are just some of the many problems affecting this kind of simulations. Not to mention the requirement of time and spatial resolutions for complex, three-dimensional and unsteady problems which can easily make the computational burden unsustainable. In this context, any prediction of cavitation noise should be strictly contextualized and assessed with a *critical eye*, being aware that (at present) even the most sophisticated CFD solvers are unable to provide a realis-

tic description of a 3D cavitating flow for acoustic purposes. The sheet cavitation is one of the most common phenomenon for a propeller and among those that can be modeled in a rather accurate way. It consists of the occurrence of a region of vapor on the blade surface which grows up and then progressively decreases in size, approximately remaining at the same position relative to the blade, as it were attached to the surface itself. Numerically speaking, these features are very “desirable”. By renouncing to any additional information about the external flow, in fact, the cavitation can be successfully modeled by a boundary element method (BEM), whose computing efficiency is incomparably higher with respect to any other Navier-Stokes based approach. On the other hand, if the bubble smoothly reduces in size on the blade surface (so that no detachment and/or no abrupt collapsing stage take place), the noise induced by cavitation should not be highly affected by compressibility effects and estimable by surface source’s contribution only. In a hydroacoustic solver based on the Ffowcs Williams-Hawkings equation, this means that the main effects of a sheet cavitation on the far-field noise should be substantially related to the linear source terms, provided that the occurrence and time-evolution of the bubble is taken into account properly. In this paper, the sheet cavitation noise is assessed for a typical, isolated marine propeller, by using the numerical approach described in [1]: the acoustic integrals are computed on a time-dependent integration manifold corresponding to the blade *plus* the bubble and the main features of the resulting noise field are discussed both in time and frequency domain.

2. Theoretical and Numerical approaches

Since our analysis is focused on noise prediction, we will avoid any description of the hydrodynamic aspects of the problem and the BEM methodology for cavitating flows. The reader can find a lot of books and papers on the matter (useful references are, for example, [2, 3]). What is important to remind here is that the BEM code is based on an incompressible, unsteady 3D formulation and is able to provide both the blade pressure distribution within the revolution period and the time-evolution of the size and shape of bubble possibly occurring on the body surface. The parameter used to trigger the cavitation is the cavitation number

$$\sigma_n = \frac{p_\infty - p_v}{\frac{1}{2}\rho(nD)^2} = -C_p|_{p=p_v}$$

where p_v is the vapor pressure. When σ_n (and then the pressure of the undisturbed medium p_∞) is set to a high value, no point upon the blade surface can reach the critical p_v value and the cavitation is avoided; alternatively, by reducing σ_n (and then p_∞ , at the fixed rotational velocity n), p may locally fall down to the vapor pressure and the model simulates the occurrence of a sheet cavity.

The Ffowcs Williams-Hawkings [4] equation is a rearrangement of the conservation laws of mass and momentum which governs the sound generated by a body moving in a fluid:

$$\mathbb{D}^2 \hat{p}(\mathbf{x}, t) = \frac{\bar{\partial}}{\partial t} \{[\rho_0 v_n + \rho(u_n - v_n)]\delta(f)\} - \frac{\bar{\partial}}{\partial x_i} \{[\Delta P_{ij} n_j + \rho u_i(u_n - v_n)]\delta(f)\} + \frac{\bar{\partial}}{\partial x_i \partial x_j} \{T_{ij} H(f)\},$$

where \hat{p} denotes the acoustic pressure disturbance and $\mathbb{D}^2 = \frac{1}{c_0^2} \frac{\bar{\partial}^2}{\partial t^2} - \bar{\nabla}^2$ is the D'Alembert operator. The equation $f = 0$ uses an implicit function to describe an arbitrary surface, u_i and v_i represent the fluid and surface velocity components respectively, $\tilde{\rho} = \rho - \rho_0$ is the density perturbation with respect to the undisturbed medium and the subscript n denotes the projection along the outward normal to the surface. In the Lighthill tensor $T_{ij} = \rho u_i u_j + P_{ij} - c_0^2 \tilde{\rho} \delta_{ij}$, c_0 is the sound speed in the undisturbed medium, P_{ij} represents the compressive stress tensor and $\Delta P_{ij} = P_{ij} - p_0 \delta_{ij}$, being δ_{ij} the Kronecker symbol. As it is well-known, the first two terms on the right-hand side are linear and known as *thickness* and *loading* noise components: the presence of the delta function $\delta(f)$ indicates that they are strictly related to the body surface and, in fact, they account

for the noise induced by the shape and the aero/hydro-dynamic loads acting on the surface of the moving body, respectively. The third source term, on the contrary, is called *quadrupole* noise and accounts for all possible (nonlinear) noise sources occurring in the flow, due to body motion. As mentioned in the introduction, the present analysis does not include this contribution and is limited to the assessment of the main hydroacoustic effects induced by the appearance and time evolution of a blade-attached bubble. This allows to use the BEM hydrodynamic model and, at the same time, to neglect any contribution from the *flow* quadrupole sources. By the Green's function approach the FWH equation is turned into an integral form, suitable for numerical implementations. In the classic *formulation 1A* (developed by Farassat, [5]), the pressure at point \mathbf{x} and observer time t is given by 2D integrals where the integration domain S is the surface of the moving body. In order to account for the presence of the bubble, however, we will adopt here the following replacement

$$\int_S \left[\frac{Q(\mathbf{y}, \tau)}{r|1 - M_r|} \right]_{\tau} dS \Rightarrow \int_S \left[\frac{Q(\mathbf{y}, \tau)}{r|1 - M_r|} \right]_{\tau} d\mathcal{S}.$$

Here \mathbf{y} is the source position, τ the emission time, $r = |\mathbf{x}(t) - \mathbf{y}(\tau)|$ the source-observer distance, M_r the projection of the rotational Mach number along $\hat{\mathbf{r}}$, Q generally indicates a function depending on the source term and $\mathcal{S} = \mathcal{S}(t)$ is now a time-dependent domain corresponding to the blade plus the bubble surface. At each time step, the coordinates of the computational nodes representing this new manifold are provided by the BEM solver. It is worth pointing out that the BEM code has to use a prescribed, not uniform inflow to give rise to an unsteady cavity, appearing and disappearing in a fixed azimuth range of the revolution period; nevertheless, the regime solution is periodic and repeats at each rotation of the blade, so the noise calculations are limited to one period.

3. Results

The analysis refers to a scaled INSEAN E779A marine propeller, a device for which a lot of experimental tests are available (although not concerning noise measurements) and is often used to validate hydrodynamic codes. A sketch of this four-bladed propeller (with a diameter $D = 0.227m$) is reported in the left figure 1.

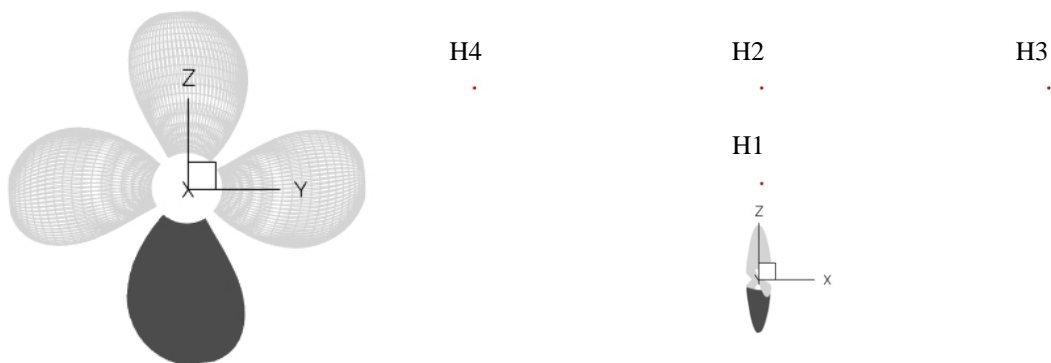


Figure 1. E779A propeller (left) and the hydrophones used for noise predictions (right).

Our calculations are limited to a single blade rotating at $n = 25rps$, at an advance ratio $J = 0.9$. The BEM code uses a 73×19 mesh and the solution is provided at 200 time steps ($\Delta\psi = 1.8^\circ$). In order to better appreciate the noise induced by cavitation and to check the reliability of the acoustic computations, a non cavitating condition is first analyzed, by placing four hydrophones in the proximity of the body (right figure 1). Points H1 and H2 are located in the disk plane, at a distance of $1R$ and $3R$ from the blade tip, respectively, while H3 and H4 concern the downstream and upstream regions, at $5R$ from the disk (being R the propeller radius).

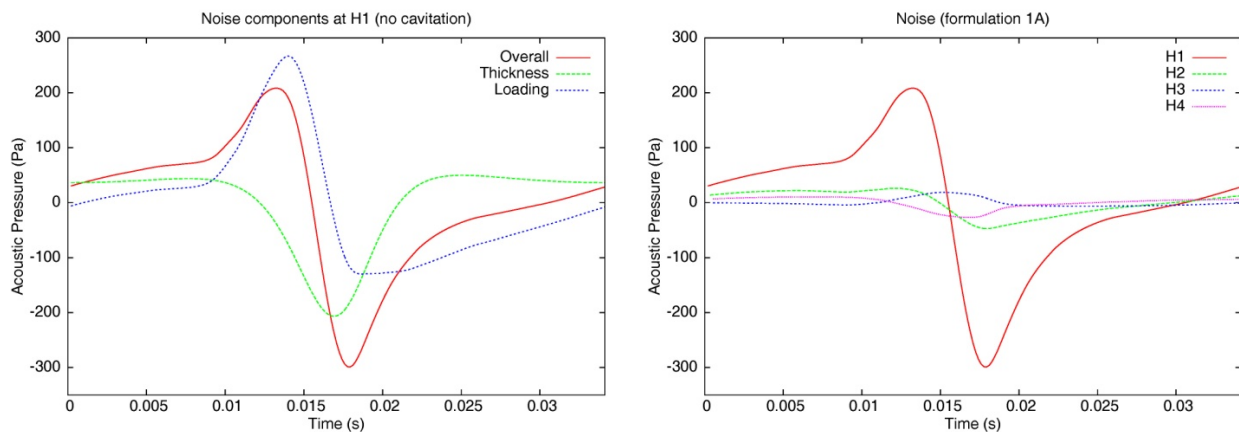


Figure 2. FWH linear noise components at point H1 (left) and the overall noise predictions at the four hydrophones reported in the figure 1 (right).

Figure 2 shows the corresponding noise predictions achieved by the linear formulation 1A. The rather “classic” waveforms of the FWH linear terms at point H1 (on the left) are exactly what we expect, and the relevant contribution from the thickness term is due to the closeness of the measurement point to the body source. Due to the geometrical features of the blade, moving far from the propeller the noise from linear terms rapidly decreases [6, 7]. In any case, the signatures at points H3 and H4 somehow respect the expected trend of the pressure signal, with a negative peak value caused by the upstream region (suction side) and a positive peak related to the downstream one (pressure side). These results provide confidence about the reliability of the FWH-based solver and, above all, give a useful reference to assess the acoustic effects induced by the sheet cavitation.

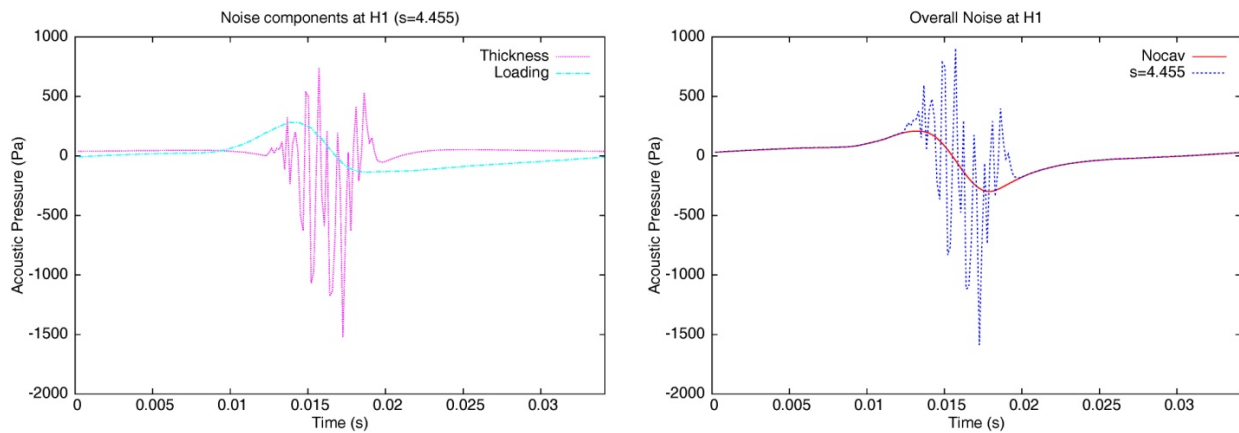


Figure 3. The noise components at point H1 (left) in presence of cavitation ($\sigma_n = 4.455$) and the comparison of the overall noise signature with and without cavitation (right).

Now let’s focus our attention on point H1 and a sheet cavitating condition ($\sigma_n = 4.455$), by computing the acoustic integrals on the corresponding domain \mathcal{S} . Figure 3 (on the left) shows the computed FWH linear source terms: as expected, the loading noise is, in practice, unaltered by the occurrence of the sheet cavity, while the thickness term exhibits a highly fluctuating waveform. At a first glance, however, this behavior appears to be more of numerical rather than physical nature and the determined increase of the acoustic pressure with respect to non cavitating condition (reported on the right picture) seems, in essence, unreliable. It could be possible to filter the overall signature, turning it into the frequency domain and cutting away the higher frequencies, but this strategy would be too much artificial, since no indication exists about which and how many frequencies should be removed. On the other hand, the main responsible of these oscillations is the

unsmooth behavior of the sheet cavity time evolution, due to the time and spatial resolution of the hydrodynamic simulation and, above all, the intrinsic limits of the numerical model. These irregularities are shown in the bubble volume time history $V_b(t)$ within the revolution period, reported in the left picture of figure 4. At about $t = 0.0124$ a cavity appears on the blade surface: its volume rapidly increases, reaches the maximum value (at $t = 0.016$) and then reduces in even a steeper way, up to completely disappear. In spite of this globally regular trend, the numerical fluctuations in the $V_b(t)$ curve heavily affect the subsequent prediction of the thickness term, whose integral kernel includes the time derivative of the unit normal vector on the \mathbb{S} surface. This explains the unreliable waveform of the resulting signature. A smart filter on such an undesirable behavior can be achieved by smoothing in time the trajectories of the computational points representing the cavity. The procedure is very simple: any spatial coordinate of a mesh point on the bubble surface at time t (indicated by x_t) is regularized with respect to the previous and next time steps, according to

$$x_t^f = \mathcal{R}_1^{N_f} \left(\frac{1}{4}x_{t-1} + \frac{1}{2}x_t + \frac{1}{4}x_{t+1} \right),$$

where x_t^f is the new “filtered” coordinate and the symbol $\mathcal{R}_1^{N_f}$ reminds that the averaging procedure is repeated N_f times. Of course, this parameter plays a relevant role: the higher N_f , the smoother and free from any numerical fluctuation the volume time history. In this case, however, an estimation of how N_f affects the reliability of the final result may be achieved by determining the change of the bubble volume with respect to the original BEM solution. The center and right pictures of figure 4 show the filtered $V_b(t)$ for $N_f = 5$ and $N_f = 9$: note how the fluctuations progressively disappear, though the general trend of the curve is preserved. Table 1 reports the percentage bubble volume variations: $\overline{\Delta V_b}$ represents the global change within the revolution period (with respect to the unfiltered volume), while ΔV_b^{max} is the maximum variation occurring at the peak value. Then, by setting $N_f = 9$, it is possible to remove most of the numerical fluctuations on $V_b(t)$ with a reduction of only 2.15% of the volume originally determined by the BEM solver in the period.

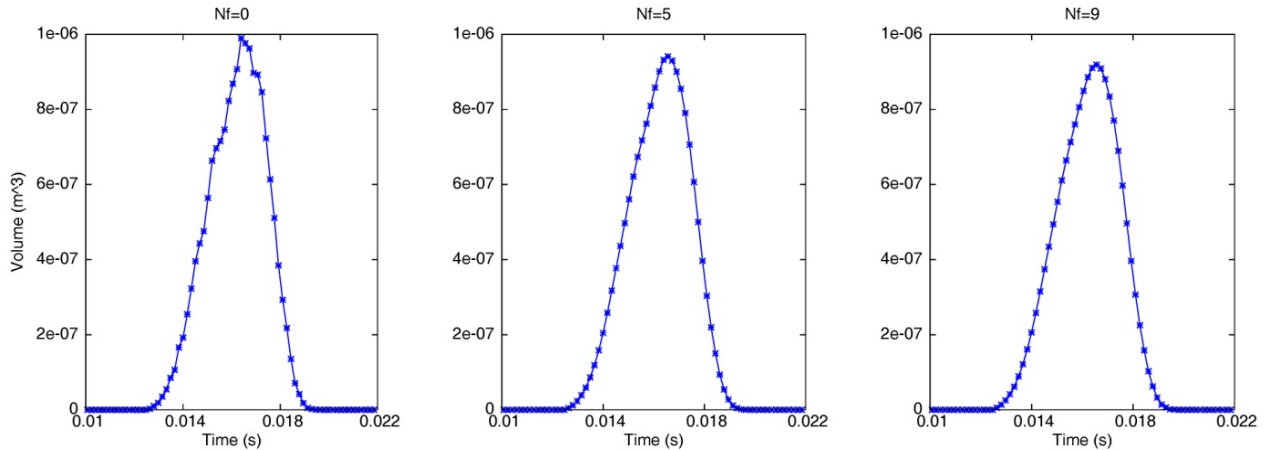


Figure 4. Volume bubble time evolution for $\sigma_n = 4.455$, as determined by the BEM code (left) and filtered by the described procedure, setting $N_f = 5$ (center) and $N_f = 9$ (right).

Table 1. Percentage bubble volume variations due to the adopted filtering procedure.

Filtering	$\overline{\Delta V_b}$ (%)	ΔV_b^{max} (%)
$N_f = 5$	1.20	5.88
$N_f = 9$	2.15	8.01

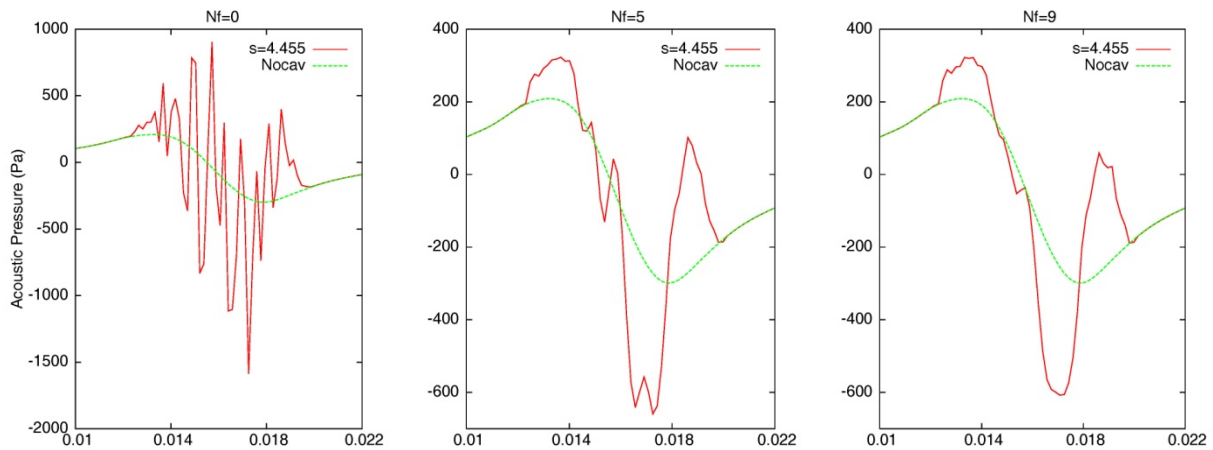


Figure 5. Cavitation noise predictions at H1 for $\sigma_n = 4.455$, as determined by the linear FWH code, not filtered (left) and filtered by the described procedure: $N_f = 5$ (center) and $N_f = 9$ (right).

Figure 5 shows how the filter acts on the resulting noise prediction at H1, here zoomed in the cavitation time window of 120 milliseconds. The fluctuations affecting the signal provided by the original BEM data (on the left) are drastically reduced and the comparison with the non cavitating conditions now appears much more coherent with the hydrodynamic result. Note how turning N_f from 5 (center picture) to 9 (right picture), the global waveform and, above all, the pressure range (now between $-600Pa$ and $+300Pa$) do not change, as though the filtering was actually able to reveal the main features of the noise induced by the bubble and “hidden” in the original solution. This is somehow confirmed by the left picture of figure 6, where the noise signals’ spectra are reported in terms of the multiples of the BPF (blade passage frequency): the occurrence of cavitation notably enriches the frequency content of the resulting noise and the spectra of the two results achieved with $N_f = 5$ and $N_f = 9$ are similar (at least in the meaningful range of the low and mid-frequencies).

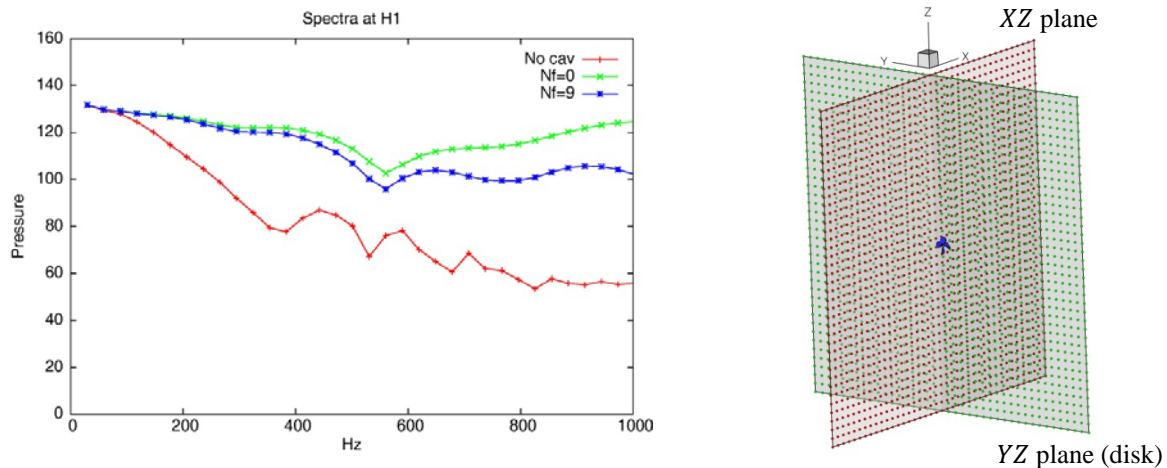


Figure 6. Signals spectra at H1 and the hydrophones (planes) used to trace the noise maps.

At this stage, let’s try to examine the general effects induced by the sheet cavitation on the hydroacoustic field. To this aim, we: *i*) compute the pressure time history at 1600 measurement points located on a prescribed plane; *ii*) turn all the resulting signals into the frequency domain through a DFT (Discrete Fourier Transform); *iii*) determine, at each point, the OASPL (OverAll Sound Pressure Level) and *iv*) trace the isocontours describing the noise map in terms of intensity and directivity. In particular, the two planes YZ and XZ are taken into account, each covering a region of $20R \times 20R$ (and barely shifted from the body in order not to intersect it). A 3D sketch of

these planes with measurement points is reported in the right picture of figure 6. The pictures in figure 7A show the computed noise maps in absence of cavitation. The FWH thickness component in the propeller disk (YZ plane, top-left picture) exhibits a uniform radiation in all directions, while the loading noise map (center picture) exhibits more stretched isocontours, depending on the prescribed not uniform inflow.

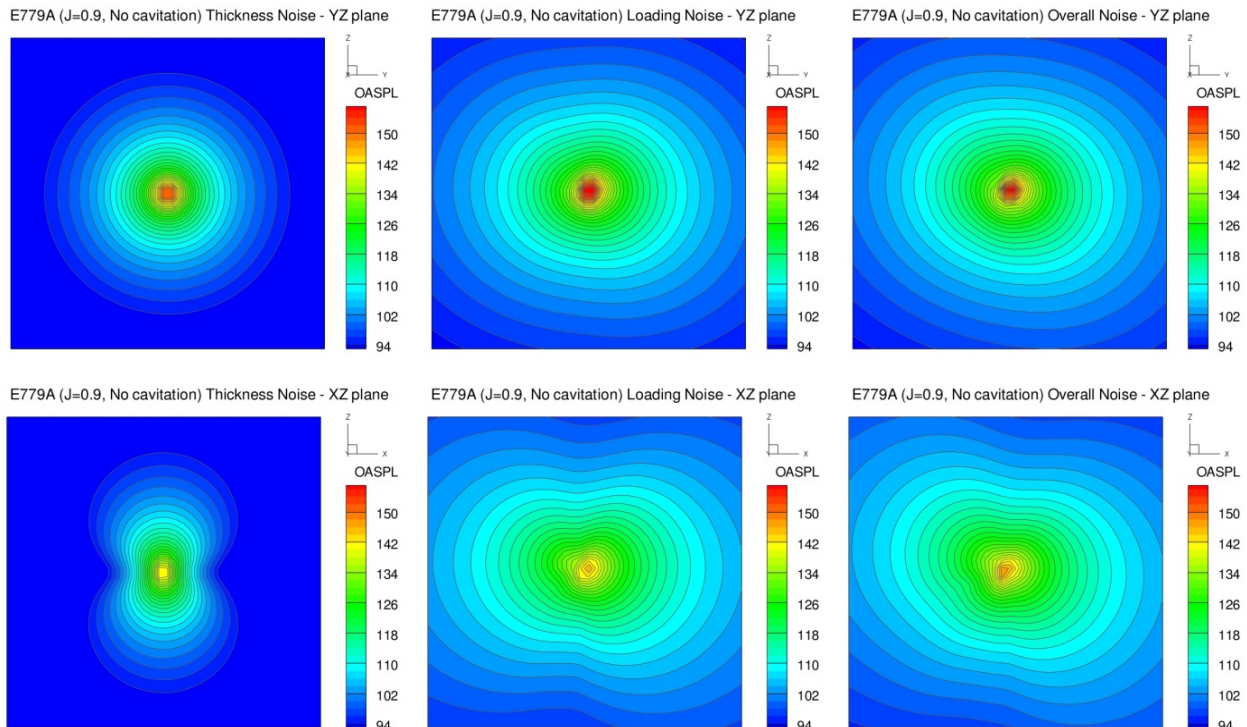


Figure 7A. Noise maps at non cavitating conditions on YZ (top) and XZ (bottom) planes.

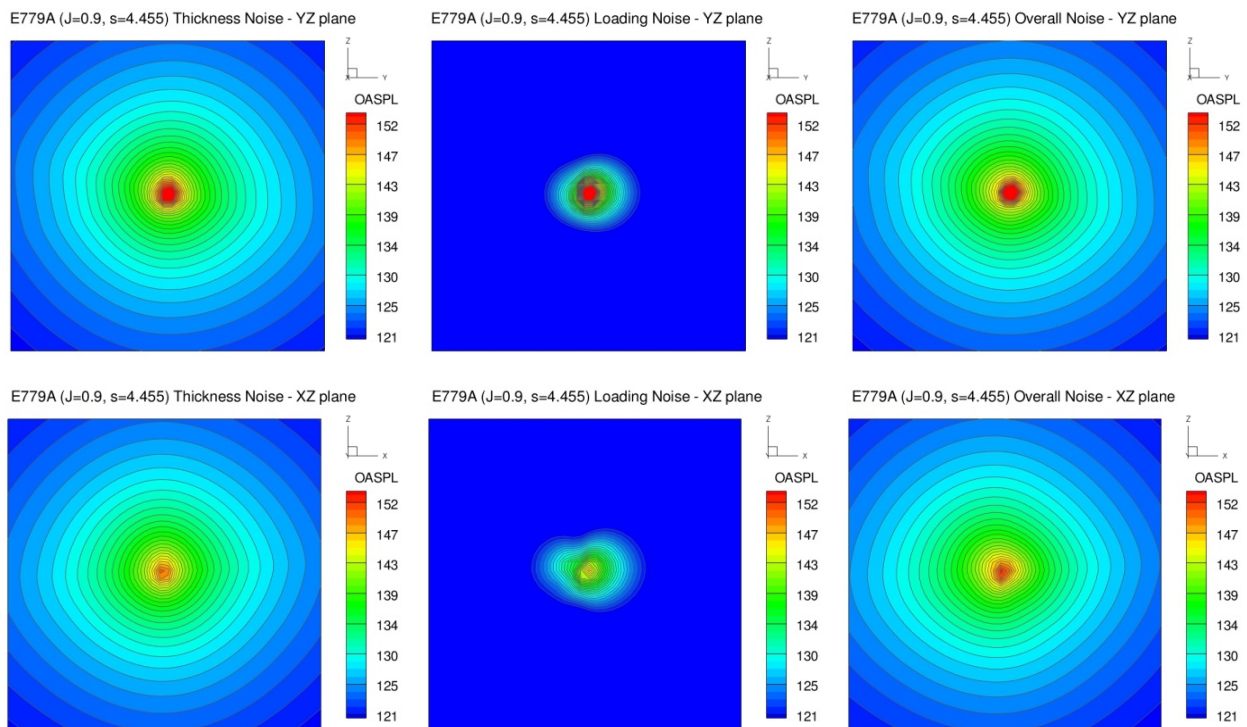


Figure 7B. Noise maps at cavitating conditions $\sigma_n = 4.455$, on YZ (top) and XZ (bottom) planes.

Nevertheless, in a plane orthogonal to the disk (XZ plane, top-left picture) the thickness is weaker and shows an evident dipole nature, with a directivity perpendicular to that of loading sources. In any case, in both planes the loading noise component represents the most relevant contribution to the overall field (right pictures) and the OASPL rapidly decreases from $150dB$ in the proximity of the blade to $94dB$ at a distance of only $20R$. The same maps are depicted in figure 7B, in presence of the sheet cavitation ($\sigma_n = 4.455$). In this case the thickness component appears as the fundamental source term insomuch as, fixing the same range of OASPL, the loading noise contribution seems to completely disappear in the far field. Furthermore, the directivity of the thickness term (and, then, of the overall noise) is now very similar to a pure monopole source. In other words, the periodic occurrence of a bubble on the blade surface makes its acoustic behavior very similar to a pulsating source, with an approximately uniform and spherical radiation. Note the values on the legends: in presence of cavitation and moving far from the propeller, the decrease of the noise level is much slower and at $20R$ from the hub the computed OASPL is still higher than $120dB$.

4. Conclusions

The numerical approach presented in this paper combines the (validated) results from a BEM methodology, concerning the modeling of a bubble occurring on the blade surface, with the robustness of the Acoustic Analogy and its own capability to deal with the different generating noise mechanisms taking place in the flow. In presence of a sheet cavity, the noise level in the far field notably increases (as well as the high-frequency content), the directivity of the acoustic field is altered and, in essence, the marine propeller behaves as a true monopole source, with a sort of uniform and omnidirectional radiation. These results are congruent with the empirical knowledge and, then, seem to be rather reliable.

Acknowledgments

This work has been developed within the frame of the research project RITMARE – The Italian Research for the Sea – coordinated by the National Research Council of Italy and funded by the Italian Ministry of Education, University and Research within the National Research Programme 2011-2013.

The author wishes to thank Dr. Francesco Salvatore for his support in providing the BEM hydrodynamic data.

REFERENCES

- [1] Salvatore F., Ianniello S., *Preliminary Results on Acoustic Modelling of Cavitating Propeller*, Computational Mechanics, Vol. 32 (4-6), 2003, pagg. 291-300.
- [2] Salvatore F., Testa C., Ianniello S., Pereira F., *Theoretical Modelling of Unsteady Cavitation and Induced Noise*, Proceedings of CAV 2006 Symposium, Wageningen, The Netherlands, September 2006.
- [3] Salvatore F., Greco L., Calcagni D., *Computational analysis of marine propeller performance and cavitation by using an inviscid-flow BEM model*, Second Int. Symposium on Marine Propulsion, SMP 2011, Hamburg, Germany, June 2011, ISBN: 978-3-86342-238-7.
- [4] Ffowcs Williams J. E., Hawkings D. L., *Sound Generation by Turbulence and Surfaces in Arbitrary Motion*, Phil. Transactions of Royal Society, 264 (A1151), 1969, pagg. 321-342.
- [5] Farassat L., *Linear Acoustic Formulas for Calculation of Rotating Blade Noise*, AIAA Journal, 19 (9), 1981, pagg. 1122-1130.
- [6] Ianniello S., Muscari R., Di Mascio A., *Ship Underwater Noise Assessment by the Acoustic Analogy. Part I: Nonlinear Analysis of a Marine Propeller in a Uniform Flow*, Journal of Marine Science & Technology, Vol. 18, 2013, pagg. 547-570.
- [7] Ianniello S., *The Underwater Noise Prediction from a Marine Propeller: an Essentially Nonlinear Problem*, 21st ICSV, Beijing, China, July 2014.